

# DEUTSCHES ELEKTRONEN – SYNCHROTRON DESY

DESY 87-144  
October 1987



## DEEP INELASTIC PHYSICS AT HERA

by

G. Ingelman

*Deutsches Elektronen-Synchrotron DESY, Hamburg*

ISSN 0418-9833

NOTKESTRASSE 85 · 2 HAMBURG 52

**DESY behält sich alle Rechte für den Fall der Schutzrechtserteilung und für die wirtschaftliche Verwertung der in diesem Bericht enthaltenen Informationen vor.**

**DESY reserves all rights for commercial use of information included in this report, especially in case of filing application for or grant of patents.**

**To be sure that your preprints are promptly included in the  
HIGH ENERGY PHYSICS INDEX,  
send them to the following address (if possible by air mail):**

**DESY  
Bibliothek  
Notkestrasse 85  
2 Hamburg 52  
Germany**

## Deep Inelastic Physics at HERA <sup>1</sup>

G. Ingelman  
Deutsches Elektronen-Synchrotron DESY  
Notkestrasse 85, D-2000 Hamburg 52, FRG

### Abstract

Basic physics and experimental aspects of deep inelastic scattering at the  $ep$  collider HERA is discussed. Kinematics and the standard electroweak cross section formalism is given. Structure functions are discussed in terms of QCD effects and possible deviations due to new physics. Experimental considerations concerning the separation of charged and neutral currents as well as kinematics reconstruction and structure function measurements are illustrated.

## 1 Introduction

Lepton-nucleon scattering has played a major rôle in our understanding of the internal structure of the nucleon. The size of the proton was first measured by electron scattering at Stanford in the mid 50's [1] and its composite, 'grainy' structure discovered with the SLAC electron beam in the late 60's [2]. Through further experiments at SLAC and the muon and neutrino beam experiments at CERN and Fermilab [3], this structure was interpreted in terms of the quark-parton model (QPM) [4]. As a result, the proton can now be well described in terms of constituent quarks bound by gluon exchange forces. A generalisation of the form-factor concept, the structure functions  $q_f(x, Q^2)$ , giving the probability to find a quark of flavour  $f$  carrying a fraction  $x$  of the proton momentum, are rather well measured by these experiments. The observed differential cross sections are in good agreement with the expectations from the electroweak theory [5]. In particular, the fractional electric charges of the quarks are thereby experimentally supported.

The squared momentum transfer,  $Q^2 = -(p_e - p_e')^2$ , between incoming and scattered lepton is the other free variable in the process. The structure functions are found to have a fundamental 'scaling' behaviour, i.e. being essentially functions of  $x$  only. The weak, scale-breaking, dependence on  $Q^2$  is of a logarithmic nature as expected from the gluon effects

<sup>1</sup>Invited talk at the XVth International Winter Meeting on Fundamental Physics, Sevilla, Spain, 23-27 February 1987.

calculable in perturbative quantum chromodynamics (QCD) [6]. Thus, not only the basic quark structure of the proton and the electroweak theory is supported by the deep inelastic scattering experiments, so is also the QCD theory of the fundamental strong interaction at the quark level.

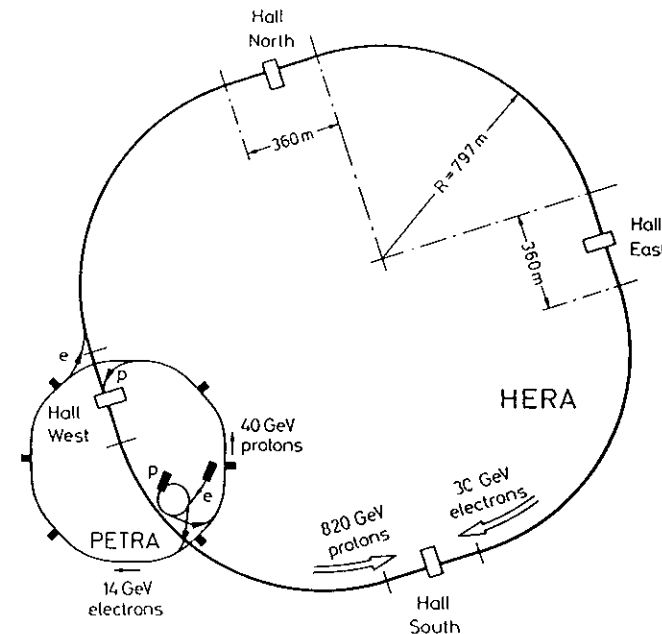


Figure 1: Layout of HERA, 'Hadron-Elektron-Ring-Anlage', with the PETRA accelerator as injector. The H1 and the ZEUS experiments will be in the north and south experimental hall, respectively.

With increasing energy, or momentum transfer, finer details in the proton structure can be investigated; the resolution scale is given by

$$d \approx \frac{2 \cdot 10^{-14}}{Q(\text{GeV})} \text{ cm.} \quad (1)$$

Although lepton beams with 2-3 times higher energy than previously available are now coming into operation at Fermilab, a substantial increase in the center-of-mass energy can only be achieved in an electron-proton collider, such as HERA now under construction at DESY in Hamburg, Fig. 1. A 30 GeV electron, or positron, beam will here collide with a 820 GeV proton beam giving a cms energy  $\sqrt{s} = 314 \text{ GeV}$ ; more than an order magnitude larger than previous fixed target experiments. The maximum momentum transfer is thus  $Q_{max}^2 = s \approx 10^5 \text{ GeV}^2$ , but is in practice limited by statistically useful event samples to  $\sim 4 \cdot 10^4 \text{ GeV}^2$ , implying a resolving power of  $\sim 10^{-16} \text{ cm}$ , eq. (1). Also the average momentum transfer is considerably

larger than the presently explored region, in charged current interactions, e.g., the mean  $Q^2$  is  $\sim 3 \cdot 10^3 \text{ GeV}^2$ . With a luminosity of  $\sim 2 \cdot 10^{31} \text{ cm}^{-2}\text{s}^{-1}$ , data samples of  $\sim 100 \text{ pb}^{-1}$  may be collected per year. Requiring at least 10 events/year in order for new processes to be observable, a 'discovery limit' of 0.1 pb is obtained. For testing the electroweak theory in detail, it is important that the electron and positron beams can be polarized. The degree of polarization that might be achieved is about 80%, but difficult problems remain to be solved concerning how to turn the transverse polarization given by the machine into the desired left- and right-handed helicity states. Two major experiments, H1 [7] (Fig. 2) and ZEUS [8], are being prepared and are expected to start their physics program in 1990.

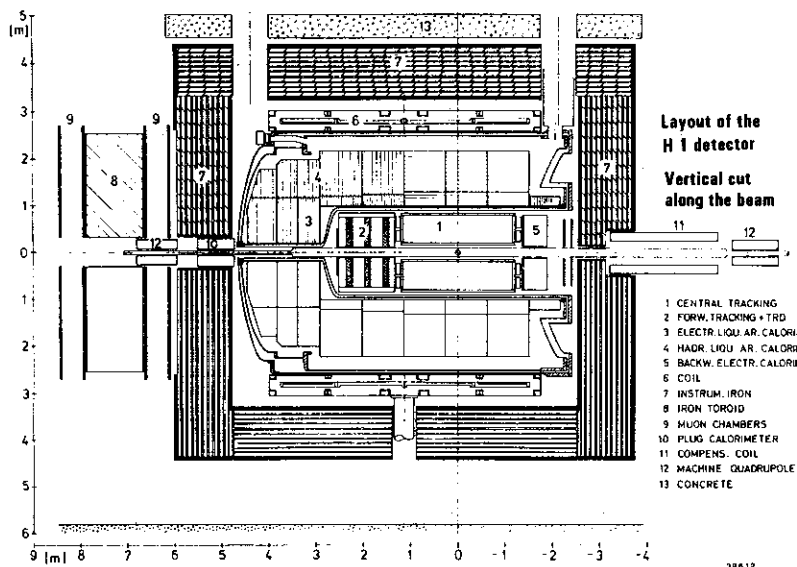


Figure 2: The H1 detector system.

The goal of the HERA experiments is to explore this new energy region in deep inelastic scattering. New, unexpected effects may be discovered. There is in any case a rich field of detailed measurements to improve our understanding of the basic interactions at the lepton-quark level. In particular, the standard electroweak model can be carefully tested in ways that are not accessible to other kinds of accelerators. In this sense, an  $ep$  collider is more of a complement than a competitor to  $e^+e^-$  and  $p\bar{p}$  colliders. In the following we will concentrate on standard physics topics, in particular the measurement of structure functions and their importance for testing QCD. New physics will only be mentioned in connection with the deviations that could be detected in the structure functions. The basic kinematics and event topology is first considered, section 2, before the theoretical aspects of cross sections and QCD effects are discussed in some detail in section 3. Some important experimental aspects are considered in section 4 and section 5, finally, contains a brief summary.

## 2 Basic event properties

The event structure obtained in an  $ep$  collider is in between the clean events produced in  $e^+e^-$  annihilation and the 'messy' ones in a  $p\bar{p}$  collider. The large difference in energy between the electron and proton beams imply that the resulting hadronic system is strongly boosted along the proton beam direction, giving a very different event topology compared to the one in the other colliding beam machines. The kinematics of the scattering is of primary importance since many physics issues, like the structure functions, are to be obtained from the differential cross sections in terms of the main kinematical variables.

### 2.1 Kinematics

The inelastic scattering process  $e + p \rightarrow \ell + H$ , where  $\ell$  is the scattered lepton and  $H$  the final hadron system, as depicted in Fig. 3a, has only two degrees of freedom. Thus, by measuring, e.g., the energy ( $E_\ell$ ) and angle ( $\theta_\ell$ ) of the scattered lepton, all other global kinematical variables can be calculated. To give the basic kinematical relations we let  $p_e$ ,  $p_\ell$  be the four-vectors of the incoming and scattered lepton, respectively, and  $P$  that of the incoming proton. The total invariant mass squared is thus

$$s \equiv (p_e + P)^2 \simeq 4E_e E_p \quad (2)$$

The ' $\simeq$ ' sign used in this section means that the masses of the electron, proton and scattered lepton are neglected; an excellent approximation at HERA energies. The exchanged vector boson,  $\gamma/Z^0$  for neutral current interactions and  $W^\pm$  for charged current interactions, has a four-vector  $q = p_e - p_\ell$  which is space-like and the momentum transfer variable  $Q^2$  defined so as to be positive,

$$Q^2 \equiv -q^2 = -(p_e - p_\ell)^2 \simeq 4E_e E_\ell \sin^2 \frac{\theta_\ell}{2} \quad (3)$$

The commonly used variable  $\nu$ , given by the relation

$$m_p \nu \equiv P \cdot q \simeq 2E_p (E_e - E_\ell \cos^2 \frac{\theta_\ell}{2}) \quad (4)$$

is the energy of the current in the target rest frame. The dimensionless scaling variables, Bjorken- $x$  and  $y$ , given by

$$x \equiv \frac{Q^2}{2P \cdot q} = \frac{Q^2}{2m_p \nu} \simeq \frac{E_e E_\ell \sin^2 \frac{\theta_\ell}{2}}{E_p (E_e - E_\ell \cos^2 \frac{\theta_\ell}{2})} \quad (5)$$

$$y \equiv \frac{P \cdot q}{P \cdot p_e} = \frac{2P \cdot q}{s} = \frac{\nu}{\nu_{max}} \simeq \frac{E_e - E_\ell \cos^2 \frac{\theta_\ell}{2}}{E_e} \quad (6)$$

are often convenient to use. Their kinematically allowed region is  $0 < x, y < 1$ , independent of energy. For the hadronization process, and also for QCD effects, an important quantity is the invariant mass,  $W$ , of the hadronic system

$$W^2 \equiv (q + P)^2 = Q^2 \frac{1-x}{x} + m_p^2 \quad (7)$$

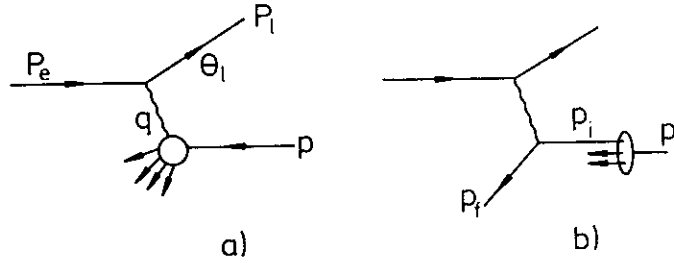


Figure 3: *Basic diagrams for deep inelastic scattering; in general (a) without assumptions about the structure of initial proton and the final hadronic system and (b) in the quark-parton model.*

The kinematic ranges of  $Q^2$  and  $W^2$  are from zero to  $s$ .

Since there are only two degrees of freedom, any two of the above variables can be used as independent variables for cross section formulae etc, but  $(x, y)$  and  $(x, Q^2)$  are the most commonly used. As mentioned, it might be preferential from the experimental point of view to use energy and angle of the scattered lepton as basic variables since they are readily measured (in neutral current events); other variables are then calculated as shown above. A more detailed account of kinematical relations in  $ep$  collisions is given in [9]. It is also important to note that so far no assumption on the structure of the proton, nor of the final hadronic state has been made. The above kinematical relations are perfectly general in that sense. By *assuming* the quark-parton model, where the current couples to a quark with four-vector  $p_i \equiv \xi(E_p, 0, 0, -E_p)$ , Fig. 3b, and *assuming* the initial and final quark to be mass-less, i.e.  $p_i^2 = p_f^2 = 0$ , one finds

$$0 = p_f^2 = (p_i + q)^2 = p_i^2 + 2p_i \cdot q + q^2 = \xi 2P \cdot q - Q^2 \Rightarrow \xi = \frac{Q^2}{2P \cdot q} \equiv x \quad (8)$$

Thus, under these assumptions, the Bjorken- $x$  variable can be interpreted as the momentum fraction,  $\xi$ , of the proton which is carried by the struck quark.

## 2.2 Phase space and event topology

The very elongated shape of the phase space for the scattered lepton and quark, shown in Fig. 4, is due to the large difference between the electron and proton beam energies. The lines are for constant  $x$  and  $Q^2$ , such that connecting the point for a given  $(x, Q^2)$  with the origin will give the momentum vector for the lepton (upper part) and current quark jet (lower part) in the lab frame; longitudinal and transverse momenta can be read off at the axes. As an example the vectors obtained for  $x = 0.5$ ,  $Q^2 = 5000 \text{ GeV}^2$  are drawn and a corresponding event with Monte Carlo generated hadrons shown in Fig. 5a. Even though the events are certainly not evenly distributed in the available phase space (see next section), they are in general very asymmetric, with most of the final state hadrons in the forward direction, i.e. along the incoming proton. This necessitates an unconventional design of the detectors, with considerably more instrumentation for tracking and calorimetry in the forward direction as is illustrated by the H1 detector in Fig. 2.

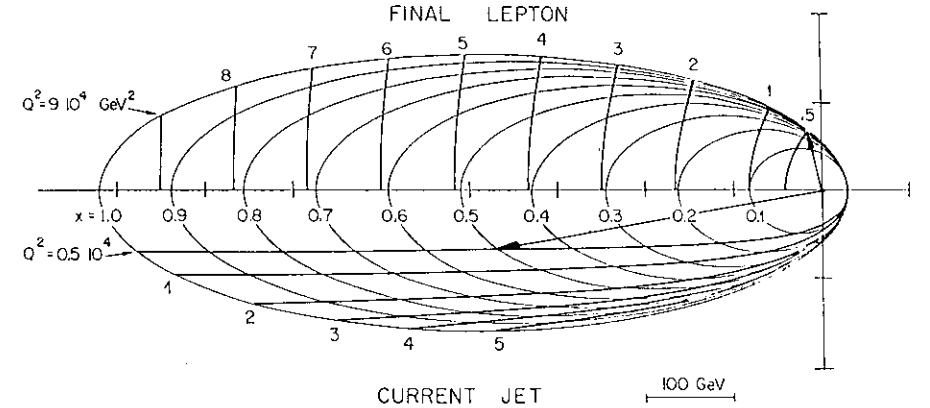


Figure 4: *Polar diagram of the kinematics for the final lepton (upper part) and the current jet (lower part) at HERA. The laboratory energy and angle is obtained by connecting a given  $(x, Q^2)$  point with the origin, as shown with the example for  $x = 0.5$ ,  $Q^2 = 5000 \text{ GeV}^2$ .*

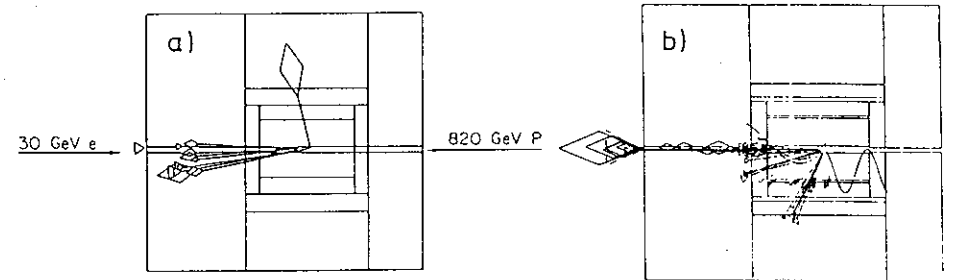


Figure 5: *Monte Carlo generated events in an idealized detector (the sizes of the diamonds and triangles give the energy of the particles). (a) Neutral current interaction with  $x = 0.5$  and  $Q^2 = 5000 \text{ GeV}^2$ , with the scattered electron upwards. (b) Charged current interaction with  $x = 0.1$ ,  $Q^2 = 5000 \text{ GeV}^2$ , note the absence of the outgoing neutrino and the extra gluon jet in the hadronic system.*

## 3 Structure functions

A main subject at an  $ep$  collider is the measurement of the proton structure functions. A detailed investigation of their variation with  $Q^2$  is an important test of QCD and deviations from the expectations might signal the occurrence of new physics effects. The extraction of the structure functions from the measured cross sections is, however, a highly non-trivial task due to the rather complex form of the differential cross section. Therefore, we must first discuss the standard electroweak theory in some detail.

### 3.1 Electroweak cross sections

The differential neutral current cross section is given by

$$\frac{d\sigma_{NC}(e^\mp)}{dx dQ^2} = \frac{4\pi\alpha^2}{xQ^4} \left[ y^2 x F_1(x, Q^2) + (1-y) F_2(x, Q^2) \pm \left( y - \frac{y^2}{2} \right) x F_3(x, Q^2) \right] \quad (9)$$

in terms of the structure functions  $F_1, F_2, F_3$ . Two of these are essentially equal through the Callan-Gross relation,  $2xF_1 = F_2$ , which holds for spin 1/2 quarks. Although there are QCD effects which violate this relation and make the longitudinal structure function nonzero, i.e.  $F_L \equiv F_2 - 2xF_1 \propto \alpha_s$ , one can usually neglect this correction (except at very small  $x$ ). More important is to take the lepton polarization into account since this is of vital importance as a tool for testing the details of the standard model. For a left- (L) and right-handed (R) electron one has

$$\frac{d\sigma(e_{L,R}^\mp)}{dx dQ^2} = \frac{2\pi\alpha^2}{xQ^4} \left[ (1 + (1-y)^2) F_2^{L,R}(x, Q^2) + (1 - (1-y)^2) x F_3^{L,R}(x, Q^2) \right] \quad (10)$$

The structure functions are given by

$$F_2^{L,R}(x, q^2) = \sum_f \left[ x q_f(x, Q^2) + x \bar{q}_f(x, Q^2) \right] A_f^{L,R}(Q^2) \quad (11)$$

$$x F_3^{L,R}(x, q^2) = \sum_f \left[ x q_f(x, Q^2) - x \bar{q}_f(x, Q^2) \right] B_f^{L,R}(Q^2) \quad (12)$$

where the sum is over all flavours  $f$  in the proton and  $q_f(\bar{q}_f)$  denote the probability to find a quark (antiquark) carrying the momentum fraction  $x$  of the proton. The coefficients for quark flavour  $f$  are given by

$$A_f^{L,R}(Q^2) = e_f^2 - 2e_f(v_e \pm a_e)v_f P_Z + (v_e \pm a_e)^2(v_f^2 + a_f^2)P_Z^2 \quad (13)$$

$$B_f^{L,R}(Q^2) = \mp 2e_f(v_e \pm a_e)a_f P_Z \pm 2(v_e \pm a_e)^2 v_f a_f P_Z^2 \quad (14)$$

where  $e_f$  is the electric charge ( $e_e = -1$ ),  $v_f = [T_{3f} - 2e_f \sin^2 \theta_W] / \sin 2\theta_W$  and  $a_f = T_{3f} / \sin 2\theta_W$  are the NC vector and axial vector couplings expressed in terms of the third component of the weak isospin ( $T_{3e} = -\frac{1}{2}$ ) and the Weinberg angle  $\theta_W$ .  $P_Z$  is the ratio of the  $\gamma$  and  $Z$  propagators

$$P_Z = \frac{Q^2}{Q^2 + M_Z^2} \quad (15)$$

The corresponding cross section for  $e_{L,R}^\pm$  is obtained from the above by the replacements

$$F_2^{L,R} \rightarrow F_2^{R,L}, \quad x F_3^{L,R} \rightarrow -x F_3^{R,L} \quad (16)$$

The pure  $\gamma$  exchange term, i.e. the one without a  $P_Z$  dependence, dominates completely at low  $Q^2$ , and the cross section then takes the familiar form measured in fixed target electron and muon beam experiments

$$\frac{d\sigma(ep)}{dx dQ^2} = \frac{2\pi\alpha^2}{xQ^4} (1 + (1-y)^2) \sum_f e_f^2 \left[ x q_f(x, Q^2) + x \bar{q}_f(x, Q^2) \right] \quad (17)$$

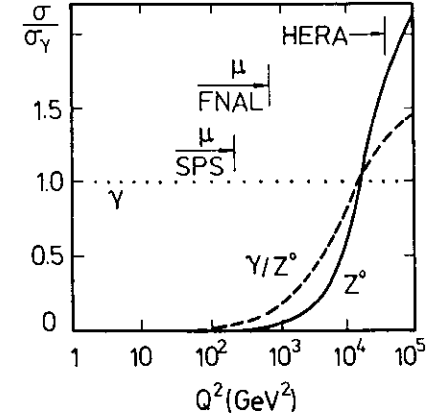


Figure 6: Relative size of the cross sections from pure  $\gamma$ , pure  $Z^0$  and their interference as a function of the momentum transfer, all normalized to the  $\gamma$ -exchange cross section. The ranges of different accelerators are also indicated.

With increasing  $Q^2$ , see Fig. 6, first the  $\gamma/Z^0$  interference term (linear in  $P_Z$ ) and then the pure weak term (quadratic in  $P_Z$ ) become important and finally dominate the cross section in the upper  $Q^2$ -range of HERA.

The differential cross sections for charged current interactions are given by

$$\frac{d\sigma_{CC}(e^-p)}{dx dQ^2} = \frac{\pi\alpha^2}{4 \sin^4 \theta_W (Q^2 + M_W^2)^2} \sum_{i,j} \left[ |V_{u,d_i}|^2 u_i(x, Q^2) + (1-y)^2 |V_{u,d_i}|^2 \bar{d}_i(x, Q^2) \right] \quad (18)$$

$$\frac{d\sigma_{CC}(e^+p)}{dx dQ^2} = \frac{\pi\alpha^2}{4 \sin^4 \theta_W (Q^2 + M_W^2)^2} \sum_{i,j} \left[ |V_{u,d_i}|^2 \bar{u}_i(x, Q^2) + (1-y)^2 |V_{u,d_i}|^2 d_i(x, Q^2) \right] \quad (19)$$

where  $V_{u,d}$  are elements of the Kobayashi-Maskawa matrix,  $u_i$  and  $d_j$  denote up-type and down-type quark flavours, respectively, and  $i, j$  are family indices. Considering only four massless quark flavours ( $u, d, s, c$ ) and using the unitarity relation  $\sum_j |V_{u,d_i}|^2 = \sum_j |V_{d,u_i}|^2 = 1$  one obtains

$$\frac{d\sigma(ep)}{dx dQ^2} \simeq \frac{G_F^2}{\pi} \left( 1 + \frac{Q^2}{M_W^2} \right)^{-2} \begin{cases} (u+c) + (1-y)^2(\bar{d} + \bar{s}) & \text{for } e_L^- \\ (\bar{u} + \bar{c}) + (1-y)^2(d + s) & \text{for } e_R^+ \\ 0 & \text{for } e_R^-, e_L^+ \end{cases} \quad (20)$$

where  $G_F = \pi\alpha/[\sqrt{2}\sin^2 \theta_W M_W^2]$  is the Fermi coupling constant,  $M_W$  the  $W$ -boson mass and  $u$  stands for the  $u$ -quark density  $u(x, Q^2)$  etc.

With the parametrizations of the quark density functions, that have been obtained from fixed target data using the QCD evolution formalism (see e.g. [10,11]) the cross section formulae give the expected event rates as shown in Fig. 7.

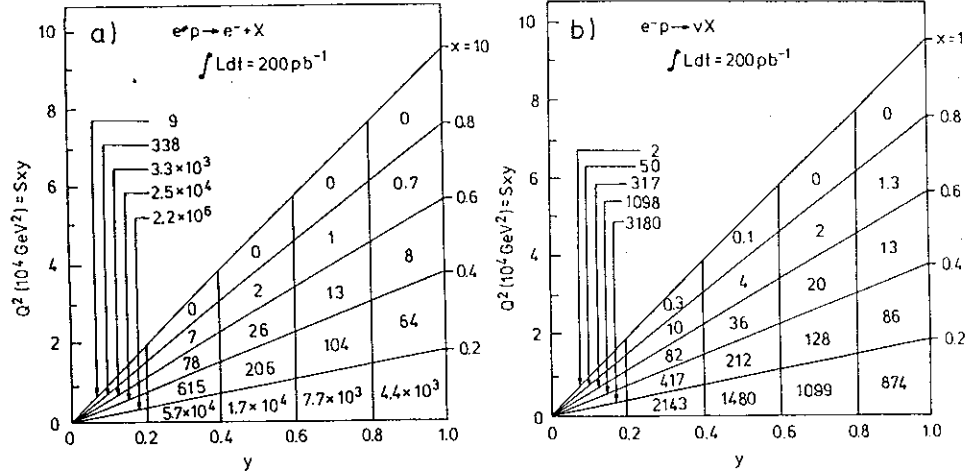


Figure 7: Event rates for neutral (a) and charged (b) current interactions with  $x, y > 0.01$  in a  $200 \text{ pb}^{-1}$  run at HERA.

### 3.2 QCD evolution

The variation with  $Q^2$  of the quark and gluon density functions are all connected through the strong interactions and are in the leading logarithm approximation given by the Altarelli-Parisi equations [6]

$$\frac{\partial q(x, Q^2)}{\partial \ln Q^2} = \frac{\alpha_s(Q^2)}{2\pi} \int_x^1 \frac{dy}{y} \left[ q(y, Q^2) P_{q \rightarrow q} \left( \frac{x}{y} \right) + g(y, Q^2) P_{g \rightarrow q} \left( \frac{x}{y} \right) \right] \quad (21)$$

$$\frac{\partial g(x, Q^2)}{\partial \ln Q^2} = \frac{\alpha_s(Q^2)}{2\pi} \int_x^1 \frac{dy}{y} \left[ q(y, Q^2) P_{q \rightarrow g} \left( \frac{x}{y} \right) + g(y, Q^2) P_{g \rightarrow g} \left( \frac{x}{y} \right) \right] \quad (22)$$

where the splitting functions

$$P_{q \rightarrow qg}(z) = \frac{4}{3} \frac{1+z^2}{1-z} \quad (23)$$

$$P_{g \rightarrow gg}(z) = 6 \frac{[1-z(1-z)]^2}{z(1-z)} \quad (24)$$

$$P_{g \rightarrow q\bar{q}}(z) = \frac{1}{2} [z^2 + (1-z)^2] \quad (25)$$

give the energy sharing in the basic QCD vertices shown in Fig. 8a. These equations simply express the fact that the parton being probed need not be an 'original' constituent, but arising through the strong interaction processes within the proton. The smaller the wavelength of the probe, i.e. the larger the  $Q^2$  of the exchanged boson, the more of such quantum fluctuations can be observed and hence the amount of quark-antiquark pairs and gluons in the 'sea' increases. Although these sea partons carry only small fractions of the proton momentum

(in an infinite momentum frame where the proton is rapidly moving) their increasing number lead to a softening of the valence quark distributions as  $Q^2$  increases.

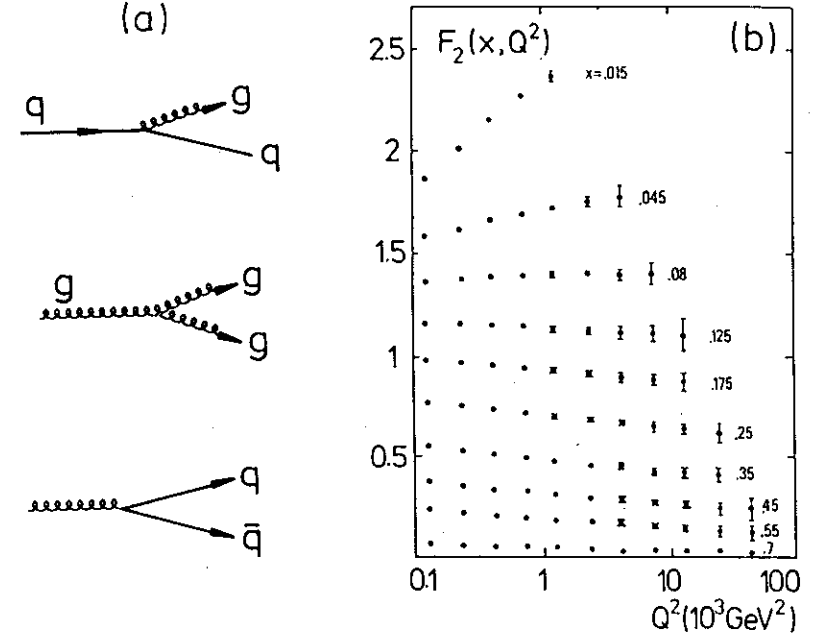


Figure 8: (a) The basic QCD vertices  $q \rightarrow q + g$ ,  $g \rightarrow g + g$  and  $g \rightarrow q + \bar{q}$ . (b) Example of QCD evolution for the  $F_2(x, Q^2)$  structure function with statistical error bars corresponding to a  $250 \text{ pb}^{-1}$  NC run at HERA.

The evolution predicted by perturbative QCD has a characteristic  $\ln Q^2$  dependence and hence the size of the effect is expected to be smaller at larger  $Q^2$ , making its verification at HERA more difficult. On the other hand, the non-perturbative effects, like higher twist operators and target mass effects which cause problems at present fixed target energies, can be neglected. Thus, the reduced magnitude of the QCD evolution effects at higher  $Q^2$ , will be compensated by the cleaner interpretation. Fig. 8b illustrates the statistical accuracy of the  $Q^2$  variation of the  $F_2$  structure function that can be obtained at HERA [12]. The example corresponds to a neutral current event sample obtainable in 150 days and is based on the QCD evolution of the simple starting distributions  $F_2(x) \sim xq(x) + x\bar{q}(x) \sim \sqrt{x}(1-x)^3$  and  $xg(x) \sim (1-x)^5$  at  $Q^2 = 3 \text{ GeV}^2$ . Thus, the statistical precision is good enough, but the question of systematic errors remains and will be discussed in next section.

The basic variation with  $Q^2$  of the strong coupling constant is given in first order QCD by

$$\alpha_s(Q^2) = \frac{12\pi}{(33 - 2n_f) \ln(Q^2/\Lambda^2)} \quad (26)$$

in terms of the number of flavours  $n_f$  and the QCD parameter  $\Lambda$ . Although presently measured values of  $\alpha_s$  are certainly consistent with the expected logarithmic ‘running’ with  $Q^2$ , they are not precise enough to clearly demonstrate it. The larger lever arm in  $Q^2$  given by HERA should improve the situation so that the variation of  $\alpha_s$  can be measured. The measurement of  $\Lambda$  becomes harder, however, due to the lower sensitivity at larger  $Q^2$  as shown in Fig. 9.

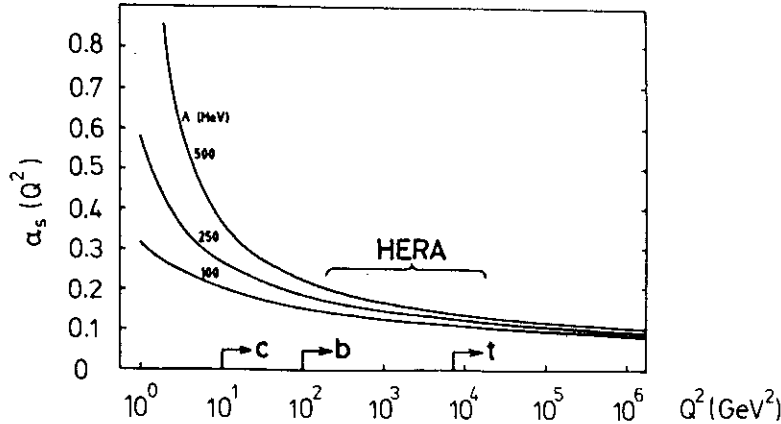


Figure 9: Variation of  $\alpha_s$  with  $Q^2$  as given by QCD for different  $\Lambda$  values. Heavy flavour thresholds are also indicated.

### 3.3 Threshold effects from heavy quarks

Passing the threshold for the production of a heavy quark will introduce an additional  $Q^2$  dependence that can obscure the genuine QCD evolution. In charged current interactions, single charm production can be obtained through Cabibbo mixing, Fig. 10a, whereas yet heavier quarks are very much suppressed through their very small mixing angles to the light quarks that occur frequently in the proton. Through the first order QCD process of boson-gluon fusion in Fig. 10b, however, all flavours can be produced without the mixing angle suppression. We illustrate this process by treating the case of photon-gluon fusion into charm,  $\gamma^* + g \rightarrow c\bar{c}$ , in some detail. Since this process is not covered by the pure electroweak cross sections of section 3.1, it gives rise to an additional term which can be written as a new contribution to the  $F_2$  structure function [11]

$$F_2^{c\bar{c}}(x, Q^2) = \frac{\alpha_s(Q^2)}{2\pi} \frac{8}{9} \int_{ax}^1 \frac{dy}{y} y g(y, Q^2) f_2^{\gamma^* \rightarrow c\bar{c}}\left(\frac{x}{y}, Q^2\right) \quad (27)$$

in terms of the probability of finding a gluon with momentum fraction  $y$  and the QCD matrix element for the photon-gluon fusion subprocess which, when integrated over the internal

degrees of freedom in the  $c\bar{c}$  system, has the form

$$f_2^{\gamma^* \rightarrow c\bar{c}}(z, Q^2) = v \left[ 4z^2(1-z) - \frac{z}{2} - \frac{2m_c^2}{Q^2} z^2(1-z) \right] + \left[ \frac{z}{2} - z^2(1-z) + \frac{2m_c^2}{Q^2} z^2(1-3z) - \frac{4m_c^4}{Q^4} z^3 \right] \ln \frac{1+v}{1-v} \quad (28)$$

where

$$v \equiv 1 - \frac{4m_c^2}{Q^2} \frac{z}{1-z} \quad (29)$$

is the velocity of the charm quark (of mass  $m_c$ ) in the subprocess cms frame. For bottom and top production in neutral currents the changes are trivial, whereas for charged currents there will be mixed heavy flavour states, like  $b\bar{t}$ , through the flavour mixing giving a somewhat different formula with two different quark masses.

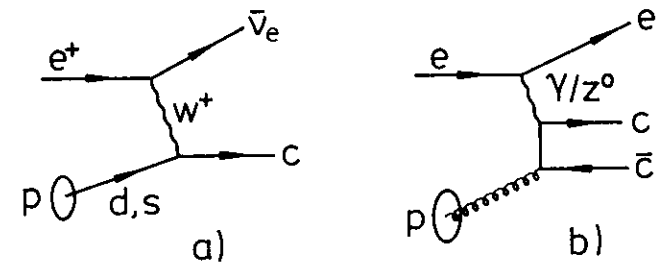


Figure 10: Charm production through Cabibbo mixing (a) and boson-gluon fusion (b).

Although the magnitude of  $F_2^{c\bar{c}}$  is small compared to the normal  $F_2$  structure function and is therefore usually neglected, its  $Q^2$ -dependence is power-like through the  $m_c^2/Q^2$  terms both in  $f_2$  and the lower integration limit in eq. (27) which is given by  $a = 1 + 4m_c^2/Q^2$ . Thus the smaller logarithmic  $Q^2$  evolution from the Altarelli-Parisi equations can be masked by this stronger power-behaviour in the threshold region, which must therefore be properly unfolded using the exact formulae above. Far above threshold, when  $m_c^2/Q^2 \ll 1$ , simpler approximate expressions can be used, e.g. one may include the charm contribution through a charm quark density distribution directly in the normal  $F_2$  structure function. (Some structure function parametrizations, e.g. [10], include parametrisations also for heavy quarks.) It has been found [13] that, in the accessible  $(x, Q^2)$ -region of HERA, the scaling violations from charm and bottom production is in practice indistinguishable from the standard leading log  $Q^2$  evolution of massless quarks, whereas top production may give non-negligible threshold effects depending on the top quark mass.

To the extent that this heavy flavour production mechanism can be tagged, e.g. by semileptonic heavy quark decays, there is also the possibility to use these processes to measure the gluon structure function in the proton.

### 3.4 Deviations due to new physics

As the name ‘structure functions’ indicate, their determination in a new domain may reveal new structures in the proton. Thus, the precision measurement of structure functions is not only important to test the QCD evolution properly, but also as a way to search for new effects through deviations from the expected behaviour. We note that, in neutral current interactions, the measurement of the scattered electron is enough to obtain the differential cross sections and thereby the structure functions. Thus, new effects also in the boson-proton vertex can be discovered in this way, i.e. without the explicit measurement of the hadronic final state. Given a signal, more information can of course be obtained when the whole final state is investigated. Many new phenomena can occur that will introduce deviations from the expected behaviour. Here, only a few possibilities of different nature will be mentioned as illustrations.

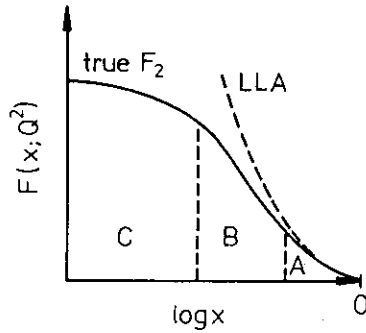


Figure 11: Illustration of the low- $x$  behaviour of the  $F_2$  structure functions in relation to new effects as discussed in the text.

The region of very low  $x$ , say  $x < 0.01$ , is a new domain not previously accessible. With HERA, values as low as  $10^{-4}$  can be reached, with  $Q^2$  still large enough to be in the deep inelastic region (see Fig. 17a). It is clear that the leading log approximation used for the structure function evolution must break down at some point, since the number of partons increases without limit as  $x$  decreases leading to an unphysical blow-up of the cross sections. This is illustrated in Fig. 11, where the true  $F_2$  structure function can be well described by the leading log approximation (LLA) in region A. For smaller  $x$ , region B, this approximation fails, but an improved perturbative calculation which takes various next-to-leading terms into account may still be adequate. For the extremely small  $x$  values in region C, estimated to be below the reach of HERA, the large number of partons can no longer be considered as free. Rather, interactions among them will be important and non-perturbative confinement effects will play a rôle. This can be intuitively understood, since the softer the parton is (i.e. the lower the  $x$ ) the larger is its corresponding wavelength and eventually it can no longer ‘fit into the bag’ of the proton. The details of such low- $x$  phenomena is, however, not well understood and is a matter of theoretical research, see e.g. [14].

The existence of new bosons that can be exchanged between leptons and quarks will lead to additional propagators, analogous to the ones from the well-known electroweak bosons.

They would result in new  $Q^2$  effects of a size that depends on the mass of the new bosons as well as the strength of their couplings to the available fermions. As with the  $W$  and  $Z$  bosons, their effect can be observed long before  $Q^2$  is above the new mass scale. Models where such new bosons arise are discussed in [15].

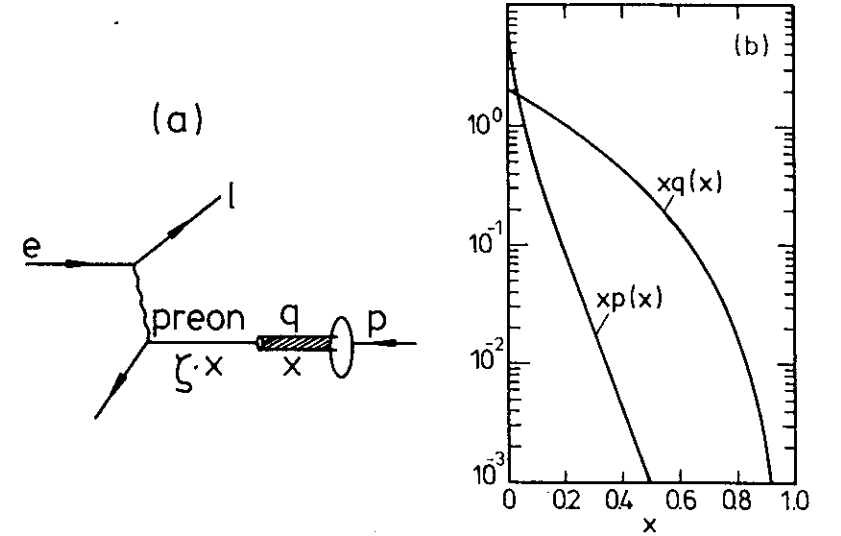


Figure 12: (a) Electron scattering off a preon constituent in a quark. (b) Comparison of the momentum distribution of quarks,  $xq(x)$ , with a possible preon distribution,  $xp(x)$ , in the nucleon.

A quark substructure may also reveal itself directly in the structure functions. If quarks are built of constituents [16], that we may call preons and which are bound by a new super-strong force at a scale  $\Lambda_{preon}$ , then for  $Q^2 > \Lambda_{preon}^2$  the boson could couple directly to these constituents, Fig. 12a. This would lead to a ‘collapse’ of the structure function in the sense that one would observe a much softer  $x$ -spectrum, as illustrated in Fig. 12b. The reason is obviously that the preon carries only a fraction,  $\xi$ , of the quark momentum, so that the proton momentum is shared by even more constituents. Limits from other experiments force the new scale  $\Lambda_{preon}$  to be at least of the order of 1 TeV, well above the HERA range. However, even for  $Q^2 < \Lambda_{preon}^2$ , deviations could be observed through so-called contact interactions [17] which are effective 4-fermion interactions in analogy with the Fermi theory for weak interactions being an effective low-energy approximation for  $W$  exchange. Some polarization asymmetries [17] are particularly sensitive to such interactions and can probe scales as large as  $\Lambda_{preon} \sim 5$  TeV corresponding to a resolving power of  $\sim 4 \cdot 10^{-16}$  cm, i.e. almost two orders of magnitude better than the ‘directly’ available resolution of  $\sim 10^{-16}$  cm derived from eq. (1) based on a maximum useful  $Q^2$  of  $\sim 4 \cdot 10^4$  GeV<sup>2</sup>.

## 4 Experimental aspects

From the discussion above, both concerning the more conventional QCD effects as well as possible exotic physics issues, the importance of precise structure function measurements should be clear. From the experimental point of view this is, however, a highly non-trivial task. For each event, the interaction must first be identified as charged or neutral current and then the kinematics reconstructed. For neutral current events the kinematical variables can be measured either from the scattered electron or from the hadronic system, whereas for the charged current events they can only be obtained from the hadronic system, which is more difficult. Events with the reconstructed  $x$  and  $Q^2$  provide the differential cross sections (assuming a known luminosity) from which the structure functions are to be extracted. Hence the quality of the result depends on the details in this chain.

### 4.1 Separation of neutral and charged current events

A main difference between neutral and charged current events is that the total transverse momentum is balanced in the former case but not in the latter due to the impossibility to measure the scattered neutrino. Thus, the vectorial sum of the transverse momenta of all particles in the event, should provide a distinction between the two classes, since ideally

$$P_{\perp} \equiv \left| \sum_i \vec{p}_{\perp i} \right| = \begin{cases} 0 & \text{in NC} \\ p_{\perp \nu} & \text{in CC} \end{cases} \quad (30)$$

The distribution,  $d\sigma/dP_{\perp}$ , of this quantity, as obtained from Monte Carlo generation of events in the region  $Q^2 > 10^3 \text{ GeV}^2$ , is shown in Fig. 13. Undetected particles in the beam holes and neutrinos from heavy flavour decays is the cause for the non-zero  $P_{\perp}$  in the NC case, whereas the scattered neutrino dominates in the CC case. It is clear that a cut in  $P_{\perp}$  at, e.g., 15 GeV will basically separate NC and CC events. The loss of true NC events will in this case be 0.31% and that of CC events 1.7%. The contamination that these losses cause in the other sample, to which they are assigned, can be obtained from the relative size of the NC and CC cross sections. Thus, the NC sample will get a contamination of  $1.7\% \cdot \sigma_{CC}/\sigma_{NC} = 0.3\%$  from CC events. Similarly, the CC sample gets a  $0.31\% \cdot \sigma_{NC}/\sigma_{CC} = 1.6\%$  contamination from neutral current events. It should be noted that, although the percentage of misassigned NC events is quite small, their contamination in the CC sample gets amplified by the much larger cross section for the neutral current interaction. The cross sections are 216 pb for NC and 43.7 pb for CC, both in the considered region  $Q^2 > 10^3 \text{ GeV}^2$ . Since the relative size of the NC and CC cross sections vary drastically with  $Q^2$ , the purity of the event samples will also vary and the above numbers on losses and contaminations should only be taken as an overall estimate. For this example a perfect detector has been assumed, only the limited coverage close to the beams has been taken into account by ignoring all particles at angles less than 70 mrad. Apparatus effects, like possible ‘holes’ in other regions and fluctuations of the calorimetric energy measurement, will be other sources of  $P_{\perp}$  imbalance and thus cause additional contaminations between the NC and CC samples.

By identifying and measuring the scattered electron, in NC events, additional criteria can be applied to improve the NC/CC separation. This does, however, require the electron to

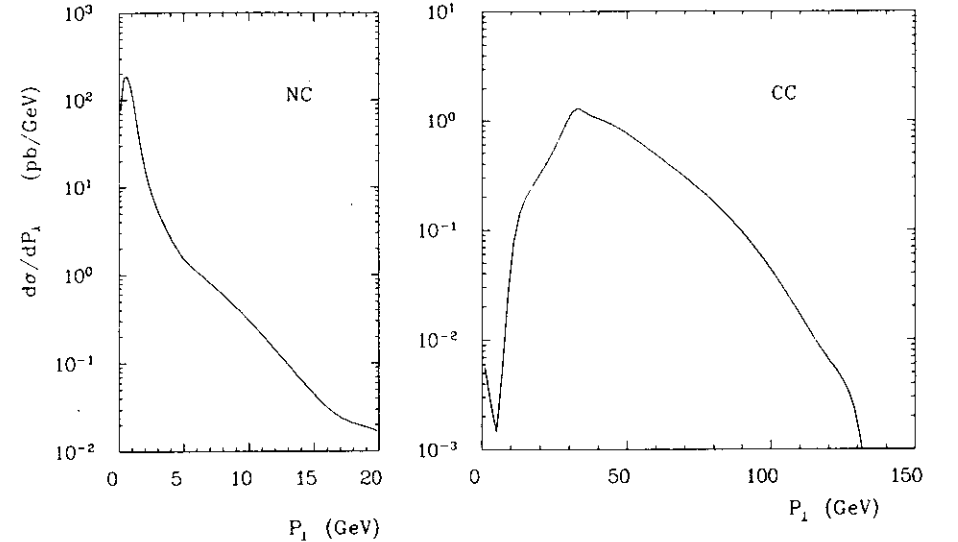


Figure 13: Distribution in total transverse momentum,  $P_{\perp}$ , in the event for neutral and charged current interactions.

be reasonably well isolated from the hadrons in the event. In principle, the electron should be well separated from the hadrons, since it is opposite in azimuth to the scattered quark jet. The quantitative result will, however, depend on how ‘noisy’ the events are, which in turn depend on the amount of gluon radiation from the incoming and scattered quark as well as the hadronization of the produced partons and the target remnant. Based on a Monte Carlo model for lepton production events [18] this can be investigated for various regions of the kinematical variables. The result is that it is only in the large- $y$  region that there is significant hadronic activity close to the electron, but in relation to the electron energy, this is still negligible, except perhaps at small  $x$ . One might expect that the smearing effects from extra gluon emission would complicate the situation, but due to the dominance of soft gluon emission there is no significant net effect. (This can be seen by comparing a model taking only first order QCD into account and a model based on parton showers (see [19] for a review) including also higher order gluon emission.) A more complete study [20] shows that the degradation of the separation due to apparatus effects is more than compensated by electron identification criteria, thus lowering the contamination to typically 0.06% and 0.8% in the NC and CC samples, respectively.

Another important observation is that the scattered electron is almost always the particle with highest  $p_{\perp}$  in the event. Thus, even without a clear identification of the electron, the highest  $p_{\perp}$  particle can be called ‘electron’ as a hypothesis, which is then cross-checked. The kinematical variables obtained from this ‘electron’ can be compared with those obtained from the remaining event (see next section) and false electron candidates thus be excluded.

## 4.2 Kinematics reconstruction

In neutral current events the kinematical variables are in principle straightforwardly obtained from the scattered lepton through eqs. (3-5). The error ellipses arising from the finite calorimeter resolution,  $\sigma_{em} = 0.15\sqrt{E}$ , is illustrated in Fig. 14a. The large errors in  $x$  at small  $y$  originate from the error propagation in the expression for  $x$

$$\frac{\partial x}{\partial E_l} = \frac{x}{y E_l} \quad (31)$$

Fig. 4 illustrates in another way the difficult regions for kinematics reconstruction, namely where lines of constant  $x$  and/or  $Q^2$  are dense.

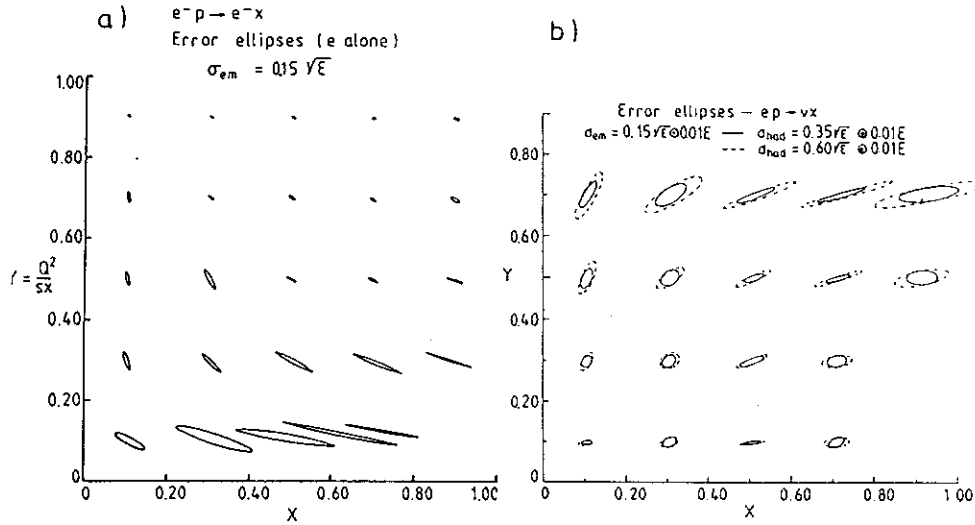


Figure 14:  $x$  and  $y$  error ellipses obtained from calorimeter measurements. (a) Electron measurement in neutral current interactions. (b) Hadron system measurement in charged current interactions, with two different energy resolutions indicated.

In charged current events the kinematics must be reconstructed from the hadronic system. In the naive QPM model, the scattered quark gives the necessary information, but in reality a number of smearing effects enter. First, the scattered quark itself is not observed but must be reconstructed from its hadronic debris, i.e. one has to rely on a jet reconstruction method and the results will depend not only on the algorithm but also to some extent on fragmentation and mass effects. Furthermore, QCD effects will make the kinematics of the hard scattering more complicated, since initial state gluon radiation may give the struck quark a large virtual mass and non-zero transverse momentum. In addition, final state parton radiation may give a set of more or less separate jets, with energy, momentum and mass difficult to measure. It is therefore important that the kinematics determination does not depend on a detailed

reconstruction of the jets in the final state, which should instead be regarded as a single system whose internal structure is of no importance.

This is achieved in the 'Jacquet-Blondel' method [21] which is based on energy momentum conservation between the invisible neutrino and the hadronic system. To show this in detail, let  $p_H$  be the four-vector of the *complete* hadronic system, i.e. the vector sum of all hadrons. The experimentally useful relations are then derived from the definition of the  $y$  variable and the fact that  $Q^2$  is given by the scattered lepton  $p_{\perp l}$  which is exactly balanced by the  $p_{\perp H}$  of the hadronic system:

$$y = \frac{P \cdot q}{P \cdot p_e} = \frac{P \cdot (p_H - P)}{P \cdot p_e} = \frac{E_p(E_H - p_{zH})}{2E_e E_p} = \frac{E_H - p_{zH}}{2E_e} = \frac{\sum_h (E_h - p_{zh})}{2E_e} \quad (32)$$

$$Q^2 = \frac{p_{\perp l}^2}{1-y} = \frac{p_{\perp H}^2}{1-y} = \frac{[\sum_h \vec{p}_{\perp h}]^2}{1-y} \quad (33)$$

The lepton and proton masses are here neglected and the incoming proton is moving in the  $+z$  direction. Clearly, this method makes no assumption on the internal structure of the incoming proton nor of the final hadron system.

The important property of these equations, as opposed to many other possibilities, is that particles along the proton direction, which are likely to be lost in the beam pipe, have a minimal influence because of their small  $E_h - p_{zh}$  and  $p_{\perp h}$ . Nevertheless, the ultimate accuracy is determined by these particle losses (as well as lost neutrinos from heavy flavour decays) and the resulting uncertainty in  $y$  and  $Q^2$  is illustrated in Fig. 15. The large errors that occur arise dominantly from kinematical configurations where the current jet is close to the beam pipe, in which case the width of the jet is very important. The wider jets resulting

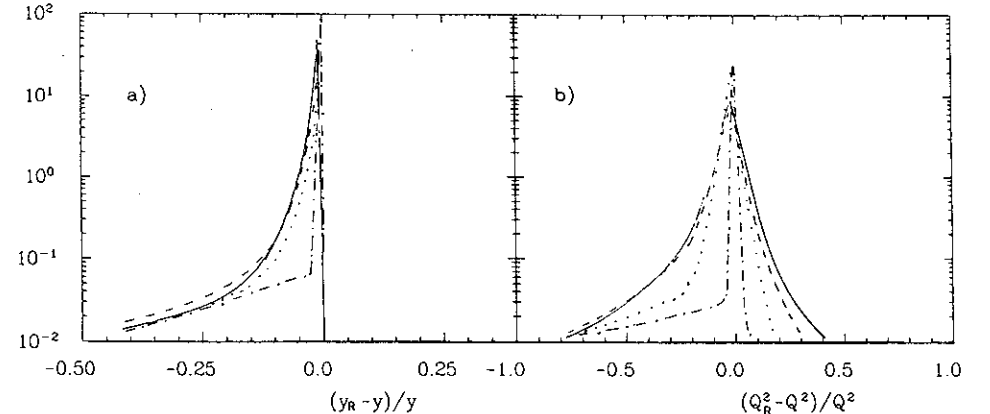


Figure 15: Relative error on  $y$  and  $Q^2$  reconstruction: due to particle losses in a 70 mrad beam hole obtained by Monte Carlo generation of HERA events ( $Q^2, W^2 > 10^3 \text{ GeV}^2$ ) in different models: quark-parton model (dotted), first order QCD matrix elements (dashed) and parton shower model (full). For comparison, quark-parton model with full angular coverage (dash-dotted, tail due to neutrinos from charm etc. decays) is also shown.

from gluon emission in the QCD models [22] give larger particle losses compared to the more pencil-like jets in the QPM model, which thus underestimates the problem of kinematics reconstruction.

This example takes only the limited coverage due to the beam hole into account. In reality, additional sources of error arise through calorimeter imperfections. In practice individual particles will not be summed in eq. (32), but rather the energies in the calorimeter cells. This will introduce both fluctuations in energy as well as angular shifts due to the calorimeter segmentation. Fig. 14b shows the expected error ellipses for the  $x, y$  measurement using the ‘Jacquet-Blondel’ method on charged current events with the energy resolution of the ZEUS calorimeter taken into account [8]. It is interesting to note the complementary nature of the reconstruction from the electron and the hadronic system; when errors are large in one case, they are small in the other. This can be exploited in neutral current events to cross-check and improve the kinematics reconstruction.

### 4.3 Structure function measurements

Since the structure function measurement is based on the distribution of events in  $x$  and  $Q^2$ , the rather large errors that may occur in the kinematics reconstruction shown in the last section seem very problematic. It is important to realize, however, that the shifts arising in the kinematical variables can to a large extent be corrected for, at least as long as they are well behaved and can be properly understood from Monte Carlo studies. Nevertheless, they will influence the useful region where migration between different  $(x, Q^2)$  bins are of a tolerable magnitude and hence the applied corrections are not too large. One can thus define a ‘safe’ region in the  $x, Q^2$ -plane, where the errors in  $x$  and  $Q^2$  can to a first approximation be neglected and the precision of the structure functions are limited by the statistical accuracy and the method used for their extraction from the differential cross sections, i.e. the unfolding of the coupling and propagator factors in the cross section formulae in section 3.1.

For charged current processes the coupling and propagator appear as an overall factor in eq. (20) which can be removed to obtain some combinations of quark distributions. For example, the difference between the electron and positron cross sections

$$d\sigma(e^-p) - d\sigma(e^+p) \sim (u - \bar{u}) - (1 - y)^2(d - \bar{d}) \quad (34)$$

depends on the  $u$  and  $d$  valence quark distributions only, but in a  $y$  (or  $Q^2$ ) dependent mixture which can only be disentangled by having cross sections at different cms energies. If an isoscalar deuterium target could be used, one would obtain the total valence quark distribution by such a difference

$$d\sigma(e^-d) - d\sigma(e^+d) \sim (1 - (1 - y)^2) x(u_v + d_v) \quad (35)$$

The extraction of structure functions from the neutral current cross section is more difficult due to the more complex dependence on the  $\gamma$  and  $Z$  couplings and propagators, but assuming the electroweak theory to fix these dependences progress can be made in several ways [12,23,20]. In some kinematic regions approximations can be made in order to simplify the cross section formulae. Thus, at low  $Q^2$  where the weak contributions are negligible compared

to the pure  $\gamma$  exchange, the  $F_2$  structure function is obtained essentially directly from eq. (17). Another possibility applicable for large  $x$ , say  $x \gtrsim 0.3$ , is to neglect the sea so that the valence  $u$  and  $d$  quark structure functions can be obtained. By combining neutral current cross sections from electron and positron beams with suitable polarizations, simplified expressions can be obtained, even without approximations, and certain combinations of quark densities extracted [23]. For example, the sum and difference of the cross sections with conjugated beams will project out the sum and difference of the quark and antiquark densities

$$d\sigma(e^+, \lambda) + d\sigma(e^-, -\lambda) \sim \sum_f [q_f(x, Q^2) + \bar{q}_f(x, Q^2)] g(y; e_f, v, a, \lambda) \quad (36)$$

$$d\sigma(e^+, \lambda) - d\sigma(e^-, -\lambda) \sim \sum_f [q_f(x, Q^2) - \bar{q}_f(x, Q^2)] h(y; e_f, v, a, \lambda) \quad (37)$$

If the polarization,  $\lambda$ , can be tuned to some particular values, the functions  $g$  and  $h$  take on simplified forms [23].

In general, the extraction of separate valence and sea quark distributions requires the combination of two, or more, differential cross sections and a variation of the cms energy in order to resolve  $y$ -dependent coefficients, like in eq. (34). For this to be useful, however, the systematic problems related to the absolute normalization of different data samples must be kept small. Since the electroweak bosons do not couple directly to gluons, the gluon distribution function can only be determined indirectly, e.g. through fits to the QCD evolution of the quark distributions.

Using charged and neutral current cross sections from  $e^+$  and  $e^-$  beams one can invert the cross section formulae and solve for four quark distributions, or combinations thereof [24]. For example, the valence up-quark distribution and the singlet structure function are given by

$$u_v(x, Q^2) = f_1^{uv} \Delta^{NC} + f_2^{uv} \Delta^{CC} \quad (38)$$

$$F_s(x, Q^2) \equiv \sum_f [xq_f(x, Q^2) + x\bar{q}_f(x, Q^2)] = f_1^s \Sigma^{NC} + f_2^s \Sigma^{CC} \quad (39)$$

where  $\Sigma$  ( $\Delta$ ) is the sum (difference) of the  $e^-$  and  $e^+$  differential cross sections and the coefficients  $f_{1,2}$  are functions of  $x, Q^2$ , the electroweak couplings and the propagators. Based on Monte Carlo study [24] using event samples corresponding to 200  $pb^{-1}$  per lepton beam, the extracted structure functions are compared to the input ones [10] in Fig. 16. The errors shown are the statistical errors obtained from the number of events in each  $(x, Q^2)$  bin after propagation through the unfolding equations and are therefore influenced also by the coefficients  $f_{1,2}$ . For the valence up-quark distribution the method works, somewhat surprisingly, better at large  $Q^2$ ; the reduced statistics does not become important until  $Q^2 \gtrsim 4 \cdot 10^4$   $GeV^2$ ! The singlet structure function, which is favoured by involving only sums of cross sections, can be well extracted in the intermediate  $Q^2$  region,  $\gtrsim 10^4$   $GeV^2$ .

Equally important as the statistical precision is the possible occurrence of systematic shifts, e.g. due to an imperfect calibration of the calorimeter energy scale and the angular measurement. These have serious effects and must be kept at an absolute minimum; the energy calibration typically at the 1% level and the electron angle measurement have systematic errors smaller than  $\sim 10$  mrad. To obtain detailed quantitative results would require a proper

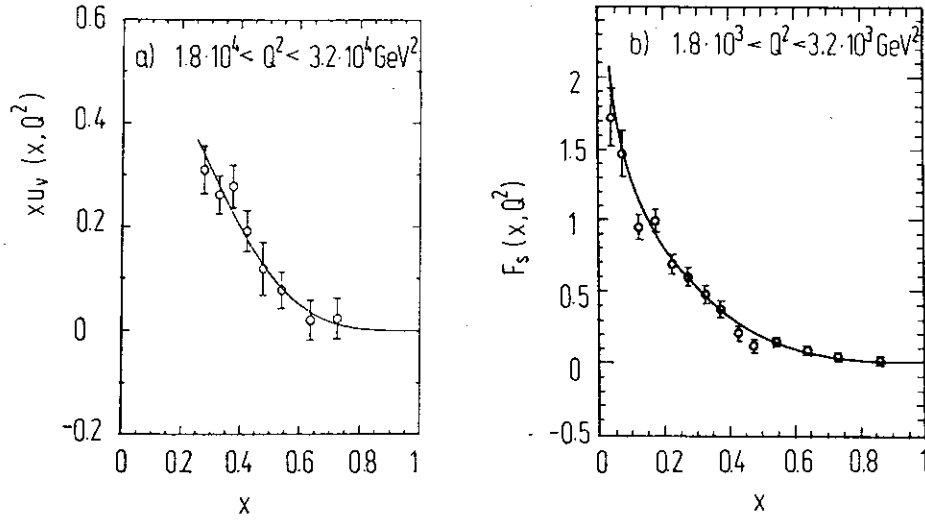


Figure 16: The valence up-quark distribution (a) and the singlet structure function (b) as reconstructed from Monte Carlo events and compared to the input form.

discussion of many experimental details, beyond the scope of this paper. This can be found in [7,8], other contributions in these proceedings and are investigated for the DESY workshop on HERA physics [20]. The region in the  $x, Q^2$ -plane which can be considered accessible for measurements, taking experimental resolution and beam hole losses into account as in the H1 experiment [7], is shown in Fig. 17. The regions considered lost due to a too large shift in the measured structure function as a result of a systematic error in the energy calibration by a few per cent are also indicated and are seen to be significant fractions of the phase space. In the neutral current case, Fig. 17a, the regions accessible through electron and ‘jet’ measurement overlap only partly. It is furthermore important to note, that there is no direct overlap with present-day fixed target neutral current measurements. Such an overlap would be important for the calibration of different experiments in the same kinematic region in order to achieve a larger lever arm in  $Q^2$  for the QCD evolution studies. This may be achieved by running HERA at a lower cms energy, e.g. a lower proton beam energy (which will make the events more symmetric and thereby easier to measure).

## 5 Summary

It is clear that  $ep$  collider physics has many interesting aspects, some of which are unique and thereby complementary to the interactions in other colliding beam facilities. HERA will be the first  $ep$  collider, and also the only one within the foreseeable future, which makes it a

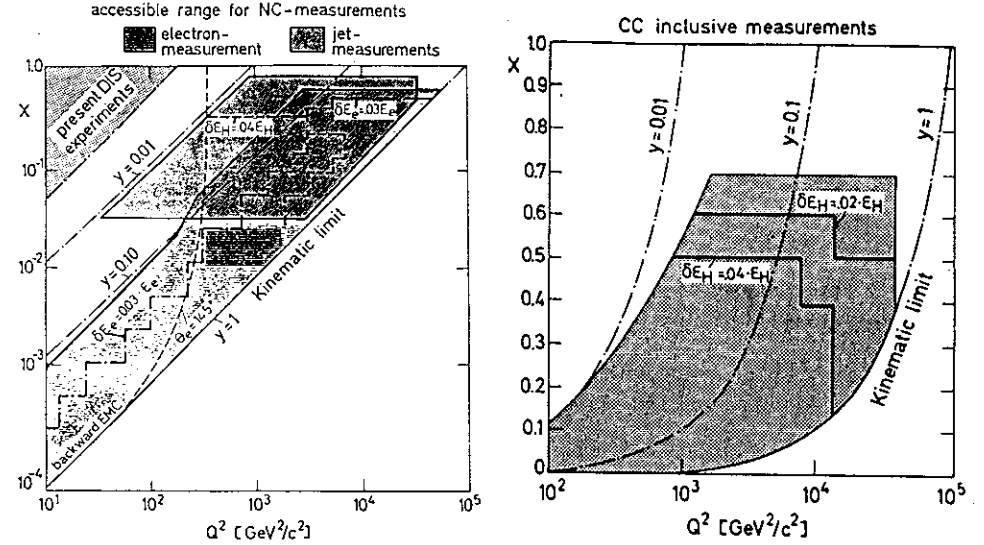


Figure 17: Accessible regions in  $(x, Q^2)$  for neutral and charged current measurements due to experimental resolution of electron/jet measurements and beam hole losses. Also shown are lines indicating a 10% shift in the measurement of the  $F_2$  structure function, due to a systematic error in the energy determination of the electron ( $\delta E_e$ ) and the hadron system ( $\delta E_H$ ).

unique adventure. The new energy and  $Q^2$  region offered will provide crucial measurements of, e.g.:

- the proton structure down to  $10^{-16}$  cm, or indirectly even  $10^{-18}$  cm
- charged and neutral current interactions for detailed tests of the standard electroweak theory
- the  $Q^2$  dependence of structure functions for a clean test of the QCD evolution equations
- jets and heavy quark production to test perturbative QCD aspects

New phenomena as predicted in some theories, or complete surprises, may occur. Standard physics issues, like structure functions, were emphasized in this paper, however. For them, it is clear that high precision measurements are required to give the desired sensitivity. Therefore, building an adequate detector and developing proper analysis techniques is certainly a big challenge.

**Acknowledgements.** I am grateful to Dr. F. Barreiro and the other organizers of the meeting for an interesting and pleasant week in Sevilla. I thank D. Haidt for a careful reading of the manuscript.

## References

- [1] R. Hofstadter, R.W. McAllister, Phys. Rev. 98 (1954) 217  
R. Hofstadter, 'Nuclear and Nucleon Structure', Frontiers in Physics, W.A. Benjamin Inc., New York 1963.
- [2] W.K.H. Panofsky, in proceedings of the XIV International Conference on High Energy Physics, Vienna, Austria 1968, (CERN scientific information service, Geneva, Switzerland 1968) p. 23  
M. Breidenbach et al., Phys. Rev. Lett. 23 (1969) 935
- [3] For a review see, e.g.  
G. West, Phys. Rep. 18C (1975) 263  
D. Haidt, H. Pietschmann, 'Electroweak Interactions - Theory and Experiment', new series of Landolt-Börnstein, in press.
- [4] R.P. Feynman, 'Photon-Hadron Interactions', Frontiers in Physics, W.A. Benjamin Inc., Reading, Massachusetts, 1972  
F.E. Close, 'An Introduction to Quarks and Partons', Academic Press, London 1980
- [5] For reviews of the electroweak theory, see e.g.  
C. Quigg, 'Gauge Theories of the Strong, Weak and Electromagnetic Interactions', Frontiers in physics, Benjamin, Reading, Massachusetts, 1983  
H. Fritzsch, P. Minkowski, Phys. Rep. 73 (1981) 67
- [6] G. Altarelli, G. Parisi, Nucl. Phys. B126 (1977) 298  
G. Altarelli, Phys. Rep. 81 (1982) 1
- [7] H1 collaboration, 'Letter of intent for an experiment at HERA', DESY June 1985  
H1 collaboration, 'Technical proposal for the H1 detector', DESY March 1986
- [8] ZEUS collaboration, letter of intent, 'ZEUS — a detector for HERA', DESY June 1985  
ZEUS collaboration, 'The ZEUS detector — technical proposal', DESY March 1986
- [9] B. Campbell, V. Elias, W.R. Frisken, Can. J. Phys. 59 (1981) 1742
- [10] E. Eichten, I. Hinchliffe, K. Lane, C. Quigg, Rev. Mod. Phys. 56 (1984) 579, *ibid.* 58 (1986) 1047
- [11] M. Glück, E. Hoffmann, E. Reya, Z. Phys. C13 (1982) 119
- [12] E. Longo, in proc. of the workshop on 'Experimentation at HERA', NIKHEF Amsterdam, 9-11 June 1983, DESY HERA 83/20
- [13] M. Glück, R.M. Godbole, E. Reya, Dortmund Univ. preprint DO-TH 87/12
- [14] L.V. Gribov, E.M. Levin, M.G. Ryskin, Phys. Rep. 100 (1983) 1
- [15] F. Cornet, DESY 87-131 and these proceedings.
- [16] For recent reviews of models of compositeness, see e.g.  
H. Harari, proc. XXIII International conf. on High Energy Physics, Berkeley 1986, Ed. S.C. Loken, World Scientific, vol. I, p. 460  
W. Buchmuller, lectures at the 1985 Schladming School, CERN-TH-4189/85 and Acta Phys. Austriaca Suppl. XXVII (1985) 517
- [17] R. Rückl, Phys. Lett. 129B (1983) 363; Nucl. Phys. B234 (1984) 91  
G. Altarelli, B. Mele, R. Rückl, proc. ECFA-CERN workshop on 'Large hadron collider in the LEP tunnel', Ed. M. Jacob, CERN report 84-10 (1984) 551  
F. Cornet, DESY 87-131 and these proceedings.
- [18] G. Ingelman, 'The Lund Monte Carlo for deep inelastic lepton-nucleon scattering — LEPTO version 5.2', DESY preprint in preparation.
- [19] G. Ingelman, 'Jets — from GeV to TeV', these proceedings.
- [20] DESY workshop on 'Physics at HERA', October 1987, proceedings to appear.
- [21] See Proceedings of the study of an *ep* facility for Europe, Ed. U. Amaldi, DESY 79/48 (1979), p. 391-394.
- [22] M. Bengtsson, G. Ingelman, T. Sjöstrand, DESY 87-097
- [23] M. Klein, T. Riemann, Z. Phys. C24 (1984) 151
- [24] G. Ingelman, R. Rückl, DESY 87-140